The 2010 IEEE/RSJ International Conference on
Intelligent Robots and Systems
October 18-22, 2010, Taipei, Taiwan

Experimental Study of Creep Response of Viscoelastic Contact Interface Under Force Control

Chia-Hung Dylan Tsai and Imin Kao
Department of Mechanical Engineering
SUNY at Stony Brook, Stony Brook, USA

Akihide Shibata, Kayo Yoshimoto,
Mitsuru Higashimori and Makoto Kaneko
Osaka University, Osaka, Japan

Abstract— **Viscoelastic materials are known to exhibit temporal response that changes force or displacement at the contact interface under position or force control, respectively. In this paper, we conduct experimental study using force control to explore and observe creep phenomenon in robotic grasping in order to better understand the nature of such contact interface, which has been widely used in soft robotic fingers, robotic feet, and contact surface of robotic arms. We found that the creep response under a constant external force exhibits the characteristics of exponentially increasing or decreasing temporal response. Such characteristics are similar in nature to those found in the *relaxation response* of viscoelastic materials when the grasping is under position control. Two different types of creep responses are found, depending on the state of grasping. Both Types I and II in creep response mirror the Types I and II in relaxation response. We also found that different loading rates under force control result in different elastic response, in addition to the temporal response. This is an interesting finding because the Fung's model postulates for an elastic response that is independent of, and can be separated from, the temporal response. The experimental results do not show such independence.**

I. INTRODUCTION

Viscoelastic materials display the properties of both solid and fluid. Most biological materials are considered viscoelastic. Two important phenomena of viscoelastic materials in contact interface are *stress relaxation* and *strain creep* under constant displacement and force, respectively. In this paper, we conduct experimental study on the creep response of viscoelastic contact interface by applying force control to deform viscoelastic material and hold the force constant in order to observe and measure the creep behavior of displacement under constant force.

A. Literature review

Study of viscoelasticity has been approached from different perspectives over the decades. The Maxwell model and the Kelvin-Voigt model are the first models being used to describe the behavior of viscoelasticity [4]. After that, the generalized Maxwell model was proposed and has been widely used in modeling of linear viscoelasticity. Sakamoto *et. al* applied the modified spring-damper model to the grasping analysis of a viscoelastic material in [15], as well as many other studies of viscoelastic behaviors presented in [14], [7], [16], [2], [13], [17], [8], [9]. Research of viscoelasticity also has been done from the rheology viewpoint in [12], [3], [1]. Golik proposed a model based on the diffusion of holes inside the rubber under an external force acted on the material [6]. Contrary to the Maxwell model which uses linear springs and dampers, Fung proposed an empirical model that separates elastic and temporal responses [5]. Tiezzi and Kao first applied Fung's model to contact interface of soft materials [19], [21], [18], [20], [11], [26], [25]. The consistency of the parameters in Fung's model has been proved in [23]. Tsai and Kao proposed a novel *latency model* which postulates that the stress relaxation can be considered as the result of uneven strain distribution before the material reaches the new equilibrium state [22]. Moreover, Tsai and Kao utilized the latency model to explain the phenomenon of the response under different loading rates by external force [24], in which different responses are shown to have been resulted from different loading rates due to the temporal effect.

B. Relaxation and creep responses of viscoelasticity

Two types of relaxations are defined in [22]. One is the Type I relaxation, exhibiting decreasing stress under a constant displacement, typically at the end of loading. The other is the Type II relaxation with increasing stress under a constant displacement, typically at the end of unloading. The other important property, creep, is the displacement/strain change when a constant force is applied to viscoelastic materials. Creep and relaxation are like two sides of a coin. They both show the delayed temporal response in either displacement or force.

C. Applications in Robotics

The study of the creep phenomenon of viscoelasticity is important because it is related to both stability and response of a contact interface. This is particularly useful when force control is employed in robotic grasping and manipulation. Furthermore, it can be used to optimize the energy consumption for robotic grasping. Understanding of the nature of viscoelastic contact interface can facilitate the modeling of robotic grasping which involves both elastic and temporal responses, such as those in soft fingers, biomedical contacts and tissues.

II. THEORETICAL BACKGROUND

As we mentioned in the previous section, creep and relaxation are both time-delayed response of viscoelasticity. Fung's model [5] is used in [23] to study the temporal

response of viscoelastic relaxation. A fundamental assumption of the Fung's model is that the elastic response and the temporal response are independent of each other and are separable. In this paper, we applied similar assumption that the elastic response and the temporal response of the displacement under force control can be separated and expressed as

$$\delta(f,t) = \mathscr{D}^{(e)}(f) \cdot h(t) \tag{1}$$

where $\delta(f,t)$ is the displacement response, f is the external force, t is the time, $\mathscr{D}^{(e)}(f)$ is the elastic response which is a function of force, and $h(t)$ is the temporal response. Based on the experimental results, we assume that the temporal response is the combination of a series of exponential terms

$$h(t) = \sum_{i=0}^{n} c_i e^{-\nu_i t} \quad \text{with} \quad \nu_0 = 0 \quad \text{and} \quad c_0 = 1 \tag{2}$$

where c_i are constant coefficients, ν_i are the exponents of the exponential function, t is time, and n is the number of terms used in the equation.

It is noted that the constant $c_0 = 1$ is assumed in equation (2), instead of $\sum_{i=0}^{n} c_i = 1$ used in Fung's relaxation model. This is an expected outcome from the latency model [22], in which the initial elastic response is affected by the inhomogeneous movement of viscoelastic materials (*e.g.* hole displacement in polymeric materials) due to latent transmission of strain across the material when subject to external stimulus. As the time approaches infinity, the temporal effect will eventually decay, leaving an asymptotic elastic response that is the true value of homogeneous stress or strain. This phenomenon can also be observed from the experimental results of relaxation in which the value of force in relaxation will eventually become the same asymptotic value, in spite of different loading rates which result in different initial forces before relaxation takes place [22]. Such results clearly illustrate that the initial values of force or displacement in the relaxation or creep response do not represent the true elastic response. The homogeneous elastic response should be the steady-state (or asymptotic) value after the temporal effect dies out. Further discussions will be presented in Section IV-C.

The response of viscoelastic materials not only is time-dependent but also depends on the strain history. Thus, an additional assumption to this model is that the materials under force/displacement start from their equilibrium configuration.

III. EXPERIMENTAL STUDY

In order to conduct experiments to measure and observe the creep phenomenon of viscoelastic contact interface, force-controlled robotic gripper is employed. The experimental setup and procedures are explained in the following sections.

A. Experimental Setup

Fig. 1 illustrates the experimental setup using a robotic parallel-jaw gripper and a high-speed camera. A grasped object is shown between the two gripper surfaces in Fig. 2.

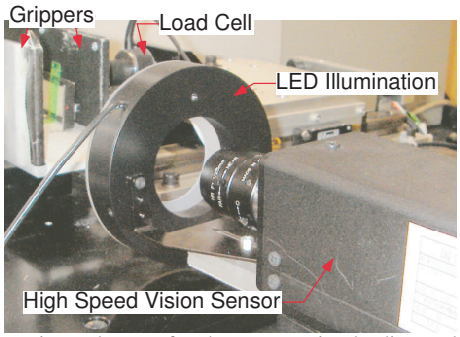

Fig. 1. Experimental setup for the compressive loading and unloading tests, showing the parallel-jaw gripper, camera, and ancillary devices

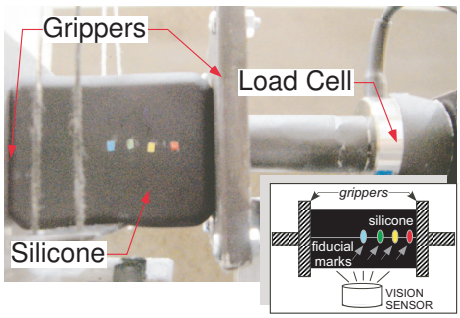

Fig. 2. Four fiducial marks with different colors are placed on the silicone object, to be tracked by a high-speed camera (or vision sensor). The black silicone block is used to eliminate the background noise when using high-speed vision camera sensor.

The grasping force is measured by the load cell mounted on the gripper that has an accuracy of $0.25N$. The accuracy of displacement of the system is $1\mu m$. The resolution of the high-speed camera is 30 Mpixel with a spatial resolution of $50\mu m$ at a frame rate of 120 fps (frame per second). A ring of LEDs is used for illumination, as shown in Fig. 1.

A rectangular parallelepiped silicone is used in the experiment with a dimension of $50mm \times 40mm \times 25mm$. Four fiducial marks of different colors are positioned on the object for the vision sensor to track the continuous movement. The silicone is dyed in black using laser toner in order to eliminate the background noise when measured by the vision camera sensor. This is shown in Fig. 2.

The mass of the gripper mounted on the load cell is $14\,g$, which moves with an acceleration up to $100\,mm/s^2$ in the experiments performed in this paper. The grasped object has much smaller movement and thus its inertial effect can be neglected. As a result, we can neglect the inertial force of the gripper and the grasped object.

B. Procedures of Experiments

The procedures of various experiments conducted under different loading rates are enumerated in the following.

1) The gripper is moved to barely touch the surface of the silicone solid. The silicone solid is supported freely by strings so that it will not fall due to gravity, but with least amount of interference to grasping in experiments. The high-speed vision sensor is calibrated with the colors of the fiducial marks on the silicone to track their positions.

2) The loading process begins with a loading rate determined *a priori* by the amount of prescribed force and the duration of holding the force after loading (for creep). Several loading rates are employed in the experiments ranging from $0.1N/sec$ to $3N/sec$.
3) When the contact force has reached the prescribed value, a PI (proportional-integral) controller is used to maintain a constant contact force for a duration of $9.5sec$. The displacement is recorded by the motion sensor mounted on the slider and the positions of the fiducial marks are tracked by the high speed vision sensor.
4) After the loading-and-hold procedure, the gripper unloads to break contacts.
5) The material rests for at least one minute before the next experiment is conducted. This one-minute rest allows for the material to restore to its original equilibrium state without affecting the subsequent experiments.

The measurements of force and displacement, as well as videos captured by high speed vision sensor are presented in the following section.

C. Experimental Results and Analysis

The results of experiments with force-controlled grasping of viscoelastic object are illustrated in Fig. 3 and Fig. 4. The figures plot experimental results based on different loading rates, and the resulting displacement of contact surface measured by the gripper (the black line in the position plot), as well as the displacements of the fiducial marks measured by the high-speed camera (the red, yellow, green, and blue colors, corresponding to the color of the fiducial marks). A low-pass Butterworth filter is utilized for conditioning the raw data obtained from load cell to filter out the high-frequency noise due to electromagnetic interference during experiments.

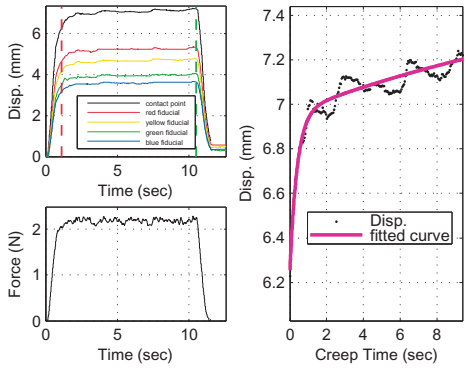

Fig. 3. The results of loading-holding-unloading experiment under a lower loading rate with force control. The loading rate is $1.96N/s$. The four lower curves of displacement correspond to the four fiducial marks in Figure 2 of the same color.

1) Different Loading Rates: Experiments with different loading rates are performed, with results plotted Figs. 3 and 4. The holding force of the experiments were maintained by a PI force feedback control algorithm at 2N. The charts on the right of Figs. 3 and 4 demonstrate the change of

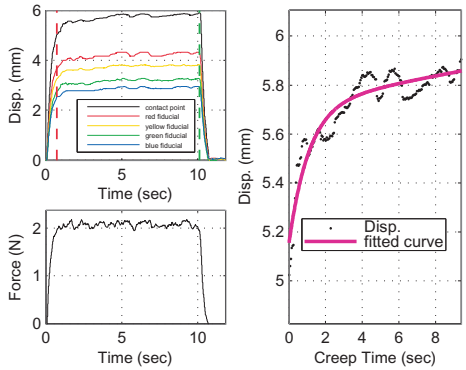

Fig. 4. The results of loading-holding-unloading experiment under a higher loading rate with force control. The loading rate is $2.71N/s$.

displacements and fitted curves based on (1) under a constant holding load. We can observe that, at begin of the holding, a lower loading rate causes a larger initial displacement, while a higher loading rate has a smaller initial rate. A further study of the effect of loading rate will be discussed in Section IV-B.

2) Repeated Loading-Holding-Unloading: Experiments are also conducted with repeated loading-holding-unloading in order to examine the response of creep due to reversed direction of loading-holding and unloading-holding. Fig. 5 and Fig. 6 present the experimental results at a lower and a higher loading rate, respectively. The upper and lower values of holding forces were set at $4N$ and $2N$, as shown in the figures. The creep phenomenon in higher loading rate is more pronounced than that in lower loading rate. Furthermore, two different types of creep are observed. Further explanation and the definition of two types of creep responses will be presented in Section IV-A

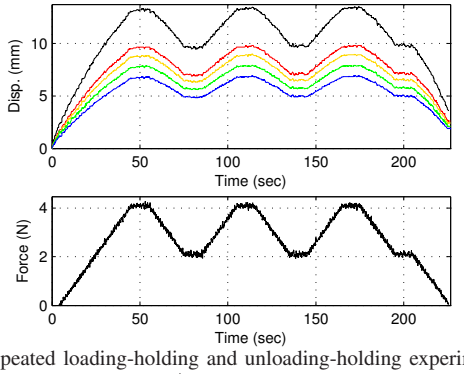

Fig. 5. Repeated loading-holding and unloading-holding experiment with a lower loading rate of $0.092N/sec$

3) Displacement Sensor vs. Vision Sensor: With the vision sensor, we can track the movement of materials away from the contact surface. The comparison shows the order of displacement in the plots. However, all four displacement curves show consistent trend of movement, including the exponential creep responses.

IV. DISCUSSIONS

Based on the preceding presentations of experimental results, some important results are discussed here.

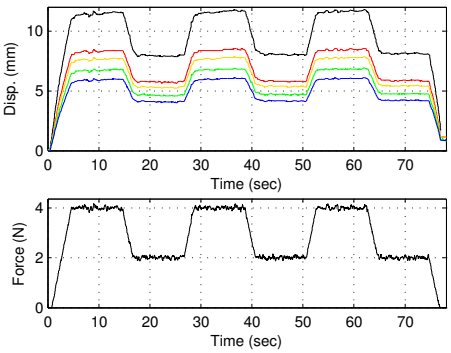

Fig. 6. Repeated loading-holding and unloading-holding experiment with a higher loading rate of $0.85N/sec$

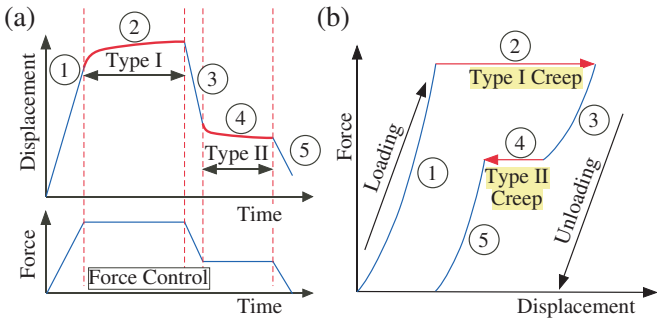

Fig. 7. Two types of creep responses under force control. (a) Type I creep is the creep under constant force after loading; while Type II creep is under constant force after partial unloading. (b) The loading and unloading curves mainly depend on the elastic property of the material. The amount of creep (horizontal red lines) depends on the speed of sound in the material. The segment numbers, 1 through 5, correspond to each other.

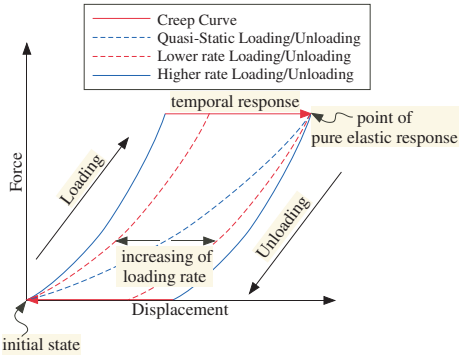

Fig. 8. The ideal loop of a force-controlled loading-holding-unloading test. Different loading rates will result in different loops. Three loops: blue dash loop, red dash loop and blue solid loop, represent three loading rates: quasi-static, a low rate and a high rate, respectively.

A. Type I and Type II Creep

Fig. 5 to Fig. 6 plot the results of experiments with repeated loading-holding and unloading-holding grasping tasks. In the figures, the displacement evolution (creep response) of the viscoelastic object depends on whether the object is under loading or unloading before holding at constant force. We defined them as Type I and Type II creep phenomena, respectively, as illustrated in Fig. 7(a).

1) The Type I creep occurs under a constant external force of compression, at the end of a loading process in segment (1) in Fig. 7(a). The Type I creep is characterized by an exponential increases in the displacement, illustrated by segment (2) in the figure. This exponential increase is partly due to the latency of temporary response as that in the relaxation [23], [22], [24]. The nature of Type II creep response gives rise to the following constraint equation in (2)

$$c_i < 0 \quad \text{for} \quad i = 1, 2, \cdots, n \tag{3}$$

2) In comparison, the Type II creep occurs under a constant external force in compression, at the end of a unloading process, represented by segment (3) in Fig. 7(a). The Type II creep is characterized by an exponential decrease in the displacement, illustrated by segment (4) in the figure. This exponential decrease is partly due to the latency of temporary response as that in the relaxation response [23], [22], [24]. The nature of Type II creep response gives rise to the following constraint equation in (2)

$$c_i > 0 \quad \text{for} \quad i = 1, 2, \cdots, n \tag{4}$$

It is noted that Type I and Type II creeps are with opposite trends of displacement evolution. This is akin to that in the Type I and Type II relaxation [23], [22], [24].

Fig. 7(b) illustrates the two types of creep responses presented in Fig. 7(a) by plotting the history of loading-holding-unloading on the force-displacement plot. The segment numbers in Fig. 7(b) correspond to those in Fig. 7(a). As can be seen in Fig. 7(b), clockwise loop is traced starting from loading, followed by Type I creep when the force is held at constant. After that, segment 3 represents partial unloading followed by Type II creep when the force is held at constant. The issue of optimization of energy consumption when performing a stable grasping task, using a force-displacement plot such as Fig. 7(b), will be a topic of our follow-up research.

B. Effect of Different Loading Rates

Fig. 8 is an illustration of the response of viscoelastic contact interface under three different loading-unloading rates, as explained in the following. The origin of the plot in Fig. 8 indicates the initial state of the material.

1) When a quasistatic loading-unloading is applied with very low loading rate, the loading and unloading curves nearly coincide with each other. The loading and unloading curves will cycle between the origin and the "point of pure elastic response" shown in Fig. 8. This is shown by the dashed blue lines.
2) If the loading-unloading rate is increased, the loading curve will shift to the left as illustrated by the green arrows shown with the "increasing of loading rate." The unloading curve will shift to the right, causing the gap between the two curves to widen to form a clockwise loop. This is shown by the dashed green lines.
3) When an even higher loading rate is applied to the material, the relationship between the grasping force and displacement will follow the blue solid curve.

When the grasping force has reached the maximum, the force is held constant. At this point, the creep will start, as indicated by the red arrow at the top of the figure moving from left to right and reaching the point at top right, indicated by the "point of pure elastic response" in the figure. When the grasping force is released, the material will follow the unloading curve until the force returns to zero. Finally, the material will slowly go back to its initial state, following the red arrow at the bottom of the loop.

Two observations are in order from Fig. 8. First, the area of the loop increases with the increase of loading rate. In other words, the energy dissipated during the operation is higher with a high loading-unloading rate in grasping. Secondly, the higher loading rate will result in a "stiffer" loading-unloading curve. This phenomenon is known as the "strain stiffening" (*or strain hardening*) effect. The higher loading rate will be accompanied by a lower value of $\mathscr{D}^{(e)}$ for the same holding force in force control experiments. Here, $\mathscr{D}^{(e)}$ can be regarded as a compliance function of the material, with lower $\mathscr{D}^{(e)}$ representing a stiffer material. Therefore, if we let $t = 0$ in (1) and (2), we will have

$$\delta(f,0) = \mathscr{D}^{(e)}(f) \cdot h(0) = \mathscr{D}^{(e)}(f) \cdot \sum_{i=0}^{n} c_i \tag{5}$$

Different value of $\mathscr{D}^{(e)}$ shows different elastic property of the material, consistent with the results presented in [24]—the higher loading rate leads to a stiffer response, also known as the *strain stiffening effect*.

C. Asymptotic Value of Displacement in Creep

Based on equation (2), the temporal response of the displacement will converge exponentially to an asymptotic value during the creep period, represented by the horizontal arrows at top and bottom of the loop in Fig. 8. When the time approaches infinity, the transient temporal response will fade out and only the elastic response, $\mathscr{D}^{(e)}$, will remain. Consequently, the point at the top right of the loop in Fig. 8 represents the pure elastic response.

$$\delta(f,\infty) = \mathscr{D}^{(e)}(f) \cdot h(\infty) = \mathscr{D}^{(e)}(f)\, c_0 = \mathscr{D}^{(e)} \tag{6}$$

We also observed that the steady-state creep response always converges to an asymptotic value regardless of the loading rate. This shows that the static state of the same input is consistent. The difference only happens when the material is in a dynamic transient state.

D. Grasp Stability with Creep Response

The time-dependent displacement response of creep under force control can significantly affect the stability of a robotic grasp. In this section, we study how the creep phenomenon can affect the grasp stability by using the friction *limit surface* [10].

Limit surface is a surface defining the stable region of tangential force and normal moment in grasping with finite area of contact. As long as the actual tangential force and normal moment fall within the region of limit surface, it will not slide; in other word, the contact is stable. The tangential friction force and moment are defined and derived in the following equations

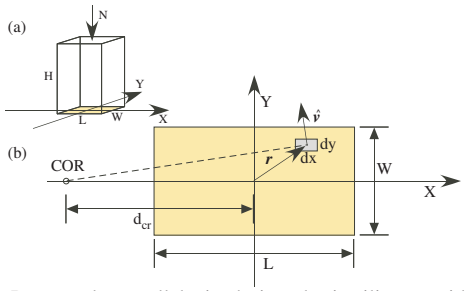

Fig. 9. (a) Rectangular parallelepiped viscoelastic silicone, with a dimensions of $L \times W \times H$. (b) The dimensions of the rectangle contact area is $L \times W$. The coordinate is centered at the center of the contact area. COR indicates the center of rotation, and d_{cr} is the distance from COR to the center of the contact area. The vector $\mathbf{r}$ is the position vector, and $\hat{\mathbf{v}}$ is the unit vector along the direction of the velocity.

$$\mathbf{f}_t = -\int\int \mu\, \hat{\mathbf{v}}\, p(x,y)\, dxdy \tag{7}$$

$$\mathbf{m}_n = -\int\int \mu [\mathbf{r} \times \hat{\mathbf{v}}] p(x,y)\, dxdy \tag{8}$$

where $\mathbf{f}_t$ is tangential force, μ is the coefficient of friction, $\hat{\mathbf{v}}$ is the unit vector of velocity, $p(x,y)$ is the pressure distribution, $\mathbf{m}_n$ is normal moment, and $\mathbf{r}$ is the position vector.

Fig. 9 illustrates the contact between a flat, rigid surface and a soft silicone material with center of rotation (COR) along x-axis. We define the unit vector along the direction of the velocity $\hat{\mathbf{v}}$ as

$$\hat{\mathbf{v}} = \frac{1}{\sqrt{(d_{cr}+x)^2 + y^2}} \begin{bmatrix} -y \\ (d_{cr}+x) \end{bmatrix}, \quad \mathbf{r} = \begin{bmatrix} x \\ y \end{bmatrix} \tag{9}$$

We apply the general pressure distribution [19] in (10) by assuming that it is only a function of x with $k = 4$.[1]

$$p(x) = C_k \frac{N}{L \times W} \left[1 - \left(\frac{x}{L} \right)^k \right]^{\frac{1}{k}} \tag{10}$$

where N is the normal force, L and W are the length and width of the contact area, C_k is a coefficient, a function of k, that adjusts the profile of pressure distribution to satisfy the equilibrium condition at the contact interface.

The limit surface can be obtained by scanning the COR along the X-axis, corresponding to the experiment. This friction limit surface with creep response is shown in Fig. 10. Since the normal force is held constant, the tangential force will not be affected by the creep phenomenon. However, due to the expansion of contact area, the margin of limit surface also expands with time, making the contact more stable. This proves that the creep phenomenon can enhance the stability of a soft contact.

[1]Hertzian pressure distribution is a special case when $k = 2$. Softer materials usually have higher values of k. As a result, we chose $k = 4$.

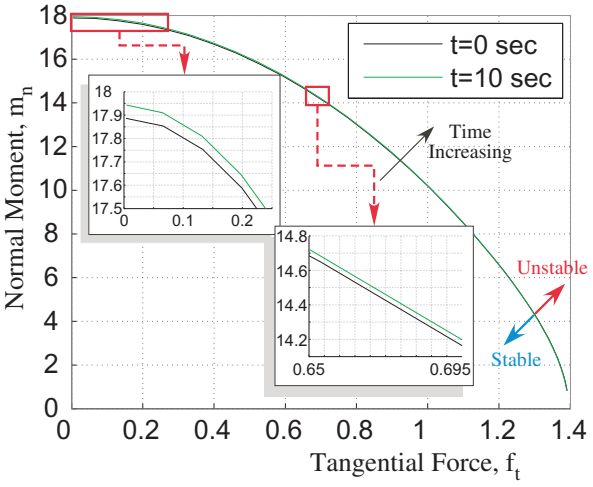

Fig. 10. Evolution of the limit surface as a function of time in the case of a constant normal force. In this analysis, we let coefficient of friction, μ, equal to 0.7, and the constant normal force, N, equal to 2N. The contact area changes based on (1) and Poisson ratio. The length of the contact area evolves from 42.22 to 42.39, and the width of the contact area evolutes from 26.38 to 26.50

V. CONCLUSIONS

In this paper, we present an experimental study to examine the creep phenomenon of viscoelastic materials using a parallel-jaw gripper under force control, equipped with a high-speed vision sensor system to track the fiducial marks located on the surface of the grasped object. We found that the creep response under constant external force features the characteristics of exponentially increasing or decreasing temporal response. Such characteristics are similar in nature to those found in relaxation of viscoelastic materials when the grasping is under position control. Two types of creep are observed, and both Types I and II in creep response mirror the Types I and II in relaxation response. In addition, it appears that different loading rates under force control result in different elastic response, $\mathscr{D}^{(e)}$. It is found that force control with creep response can enhance the stability of soft contacts. This is a subject of future investigation because the Fung's model postulates an elastic response that is separable from and independent of the temporal response.

VI. ACKNOWLEDGMENT

This research has been supported by the NSF (National Science Foundation) Grants CMS0428403 and CMMI0800241, as well as a grant from JST H19/299-1 (Japan Science and Technology Agency).

REFERENCES

[1] D. B. Adolf, R. S. Chambers, and J. Flemming. Potential energy clock model: Justification and challenging predictions. *Journal of Rheology*, 51(3):517–540, 2007.

[2] F. Barbagli, A. Frisoli, K. Salisbury, and M. Bergamasco. Simulating human fingers: a soft finger proxy model and algorithm. In *Proc. IEEE Int. Symp. on Haptic Interface, HAPTICS'04*, 2004.

[3] W. N. Findley and J. S. Y. Lay. A modified superposition principle applied to creep of non-linear viscoelastic material under abrupt changes in state of combined stress. *Trans. of the Society of Rheology*, vol. 11(3):361–380, 1967.

[4] W. Flugge. *Viscoelasticity*. Blaisdell Publishing Company, 1967.

[5] Y. C. Fung. *Biomechanics: Mechanical Properties of Living Tissues*. Springer-Verlag, 1993.

[6] A. Z. Golik and Y. F. Zabashta. a molecular model of creep and stress relaxation in crystalline polymers. *Mekhanika Polimerov*, pages 969–975, 1971.

[7] R. D. Howe, N. Popp, I. Kao, P. Akella, and M. R. Cutkosky. Grasping, manipulation, and control with tactile sensing. In *Proc. IEEE Int. Conf. on Robotics and Automation, ICRA*, Cincinnati, OH, 1990.

[8] T. Inoue and S. Hirai. Elastic model of deformable fingertip for soft-fingered manipulation. *IEEE Trans. in Robotics*, 22:1273–1279, 2006.

[9] T. Inoue and S. Hirai. Quasi-static manipulation using hemispherical soft fingertips by means of minimum d.o.f. two-fingered robotic hand. *J. of the Robotics Society of Japan*, 24:945–953, 2006.

[10] J. W. Jameson. *Analytic Techniques for Automated Grasp*. PhD thesis, Department of Mechanical Engineering, Stanford University, June 1985.

[11] I. Kao and F. Yang. Stiffness and contact mechanics for soft fingers in grasping and manipulation. *the IEEE Trans. of Robotics and Automation*, 20(1):132–135, February 2004.

[12] M. Kimura, Y. Sugiyama, S. Tomokuni, and S. Hirai. Constructing rheologically deformable virtual objects. In *Proc. IEEE Int. Conf. on Robotics and Automation, ICRA*, pages 3737–3743, 2003.

[13] Y. Li and I. Kao. A review of modeling of soft-contact fingers and stiffness control for dextrous manipulation in robotics. In *Proc. IEEE Int. Conf. on Robotics and Automation, ICRA*, pages 3055–3060, Seoul, Korea, 2001.

[14] D. T. V. Pawluk and R. D. Howe. Dynamic contact of the human fingerpad against a flat surface. *ASME Jour. of Biomechanical Engineering*, vol. 121(6):605–611, 1999.

[15] N. Sakamoto, M. Higashimori, T. Tsuji, and M. Kaneko. An optimum design of robotic hand for handling a visco-elastic object based on maxwell model. In *Proc. IEEE Int. Conf. on Robotics and Automation, ICRA 2007*, pages 1219–1225, Roma, Italy, April 10-14 2007.

[16] K. B. Shimoga and A. A. Goldenberg. Soft robotic fingertips - part I and II: A comparison of construction materials. *Int. Jour. of Robotic Research*, 15(4), 1996.

[17] H. Takagi, M. Takahashi, R. Maeda, Y. Onishi, Y. Iriye, T. Iwasaki, and Y. Hirai. Analysis of time dependent polymer deformation based on a viscoelastic model in thermal imprint process. *Microelectronic Engineering*, 85:902–906, 2008.

[18] P. Tiezzi and I. Kao. Characteristics of contact and limit surface for viscoelastic fingers. In *IEEE Int. Conf. on Robotics and Automation, ICRA 2006*, pages 1365–1370, Orlando, Florida, May 15-19 2006.

[19] P. Tiezzi and I. Kao. Modeling of viscoelastic contacts and evolution of limit surface for robotic contact interface. *IEEE Transaction on Robotics*, 23(2):206–217, April 2007.

[20] P. Tiezzi, I. Kao, and G. Vassura. Effect of layer compliance on frictional behavior of soft robotic fingers. In *Proc. IEEE Int. Conf. on Intelligent Robots and Systems (IROS 2006)*, pages 4012–4017, Beijing, China, October 2006.

[21] P. Tiezzi, I. Kao, and G. Vassura. Effect of layer compliance on frictional behavior of soft robotic fingers. *Advanced Robotics*, 21(14):1653–1670, 2007.

[22] C. D. Tsai and I. Kao. The latency model for viscoelastic contact interface in robotics: Theory and experiments. In *Proc. 2009 IEEE Int. Conf. on Robotics and Automation (ICRA 2009)*, pages 1291–1296, Kobe, Japan, May 2009.

[23] C. D. Tsai, I. Kao, N. Sakamoto, M. Higashimori, and M. Kaneko. Applying viscoelastic contact modeling to grasping task: an experimental case study. In *International Conference on Intelligent Robots and Systems, IROS*, pages 3737–3743, 2008.

[24] C. D. Tsai, I. Kao, K. Yoshimoto, M. Higashimori, and M. Kaneko. An experimental study and modeling of loading and unloading of nonlinear viscoelastic contacts. In *International Conference on Intelligent Robots and Systems, IROS*, pages 3737–3743, October 2009.

[25] N. Xydas and I. Kao. Modeling of contacts and force/moment for anthropomorphic soft fingers. In *Proc. of Int. Conf. on Intelligent Robots and Systems, IROS*, pages 488–493, Victoria, Canada, 1998.

[26] N. Xydas and I. Kao. Modeling of contact mechanics and friction limit surface for soft fingers in robotics, with experimental results. *Int. J. of Robotic Research*, 18(8):941–950, 1999.